High Torque Density Dual-stator Vernier Motors with Flux Concentrating Rotors

Esmaeil Mohammadi
e-Motion Laboratory
Department of Mechanical Engineering
University College London
London, UK
esmaeil.mohammadi.23@ucl.ac.uk

Ali Mohammadi
SPARK Laboratory
Pigman College of Engineering
University of Kentucky
Lexington KY, USA
ali.mohammadi@ieee.org

Mohammad Amin Jalali Kondelaji
e-Motion Laboratory
Department of Mechanical Engineering
University College London
London, UK
amin.jalali@ucl.ac.uk

Pedram Asef
e-Motion Laboratory
Department of Mechanical Engineering
University College London
London, UK
pedram.asef@ucl.ac.uk

Ion G. Boldea
Electrical Engineering Department
Polytechnic University of Timisoara
Timisoara, Romania
ion.boldea@upt.ro

Dan M. Ionel
SPARK Laboratory
Pigman College of Engineering
University of Kentucky
Lexington KY, USA
dan.ionel@ieee.org

***Abstract*—Axial Flux Permanent Magnet (AFPM) machines are increasingly being studied for low-speed, direct-drive applications due to their compact structure and high torque output. This study proposes two novel dual-stator AFPM vernier machine topologies: a spoke-type rotor configuration and a back-to-back Halbach array rotor. Both designs employ dual outer stators with 12 double-layer concentrated windings, and high-polarity rotor configurations to enhance flux concentration. A three-dimensional finite element model, which was previously validated by a laboratory prototype motor was utilized to evaluate the electromagnetic characteristics of the proposed topologies. These characteristics include torque density, airgap flux distribution, and harmonic content. Comparative results show that under a current density of 35 A/mm^2, the spoke-type topology achieves an efficiency of 85.2% and an average torque that is 13.5% higher than the double-stator single-rotor (DSSR) Halbach topology, which records 83.5% efficiency. Both topologies exhibit a torque ripple of 2%, highlighting consistent electromagnetic performance and smooth operation. Additionally, the spoke-type DSSR features an extended constant power operating range due to enhanced flux concentration. These findings confirm the spoke-type AFPM machine as a promising candidate for high-performance direct-drive systems, delivering improved electromagnetic torque, efficiency, and operational smoothness through strategic magnetic topology and flux profiling.**

***Index Terms*—AC machines, Axial flux motors, dual stator, finite element analysis, Halbach array, spoke rotor.**

I. Introduction

The development of high-performance electric machines has garnered significant interest in recent years. Axial Flux Permanent Magnet (AFPM) machines have been extensively studied for their high power density and efficiency, making them ideal for electric vehicles (EVs) compared to conventional electric motors [1], [2]. Among different types of rotors, surface-mounted permanent magnet (SPM) configurations suffer from pole-to-pole flux leakage, which reduces airgap flux density, while the spoke-type and Halbach designs offer distinct advantages [3]–[6]. High-polarity PM rotors, in these machines improve torque and efficiency in low-speed applications by reducing flux per pole, which allows for smaller magnetic components and and lower stator winding end-turn volume [7], [8]. This design approach contributes to compact motor geometry and improved thermal performance, especially in space-constrained environments. Additionally, it facilitates optimized electromagnetic utilization, enabling enhanced control precision and energy savings across varying load profiles [9]–[11].

Recent advancements include the triple-stator AFPM vernier machine with toroidal windings on the inner stator. This topology demonstrates exceptional torque density and power factor improvement via flux-focusing effects and compact winding arrangements, with its performance optimized through quasi-3D Finite Element Analysis (FEA) and validated by complete simulations [12]. A dual-stator alternative introduces discrete skew PM shaping to minimize cogging and torque ripple, thereby boosting output torque at low speeds. Comparative evaluations indicate that both machines offer distinct advantages in electromagnetic behavior, making them promising for industrial and automotive applications [13].

Further design efforts have focused on improving the performance of double-sided AFPM TORUS machines. Innovations include integrating skewed PMs with Halbach arrays and evaluating two design variants to identify optimal implementation strategies. Using response surface methodology for parameter optimization and 3D FEA for performance verification, researchers demonstrated substantial electromagnetic enhancements [14], [15]. Complementary studies provide deeper analytical insights. For instance, [16] developed and validated nonlinear harmonic models of Halbach-array AFPM

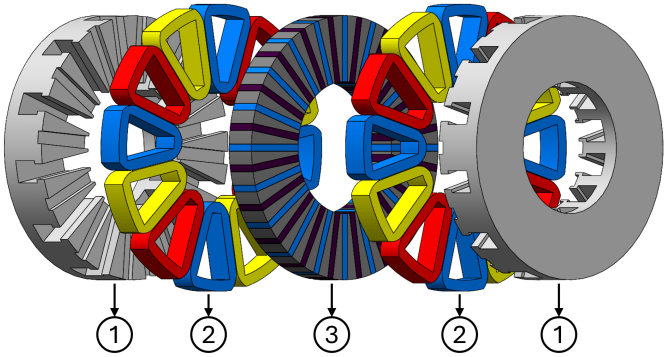

Fig. 1. Innovative construction of the spoke-type vernier machine. (1) Stators. (2) Stator winding coils. (3) Spoke-type rotor.

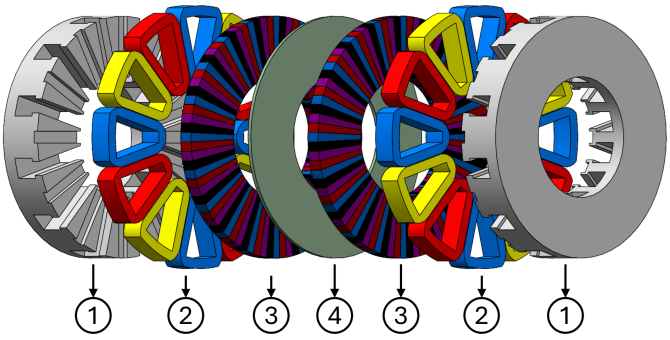

Fig. 2. Innovative construction of the back-to-back Halbach array vernier machine. (1) Stators. (2) Stator winding coils. (3) Halbach array rotor. (4) Rotor decoupler.

machines, accounting for stator saturation and dual three-phase windings. These models, presented in both Cartesian and rotor reference frames, enabled precise computation of force densities and field distribution. Similarly, [17] introduced a 3D analytical solution framework by applying magnetic scalar potential and modified Bessel functions to solve Laplace and Poisson equations. This method yielded closed-form expressions for key electromagnetic characteristics regardless of pole configuration and offered broader applicability than traditional 2D approaches. It provides valuable insights into magnetic behavior, back electromotive force (EMF) generation, torque production, and design optimization for modern AFPM machines.

This paper presents a comprehensive study and comparative analysis of two high-performance AFPM motors: one incorporating a spoke-type rotor within a dual-stator layout, and the other adopting a back-to-back Halbach array rotor design. Both architectures employ dual outer stators outfitted with double-layered three-phase windings and utilize high-polarity PM structures to enhance flux concentration and torque output.

Through 3D FEA, the electromagnetic characteristics of both machines are evaluated in detail. The findings reveal that although the spoke-type configuration necessitates a dual-stator arrangement, it demonstrates superior torque density and significantly reduced torque ripple when compared to its Halbach counterpart. These outcomes highlight the effectiveness of advanced flux-shaping strategies in optimizing AFPM topologies for low-speed, direct-drive applications.

The remainder of this paper is arranged as follows. Section II outlines a systematic and in-depth design methodology for both proposed machine. Section III presents the performance analysis, supported by a detailed comparative table to establish consistency and validate robustness across design variants. This section also includes the core discussion of results and design trade-offs. Section IV concludes the paper by summarizing the key findings and outlining the principal contributions and engineering implications.

II. Topologies and Principle of Operation

This study introduces two advanced AFPM machine topologies, the dual active stator with spoke-type rotor (Spoke-DSSR) and the dual active stator with back-to-back Halbach array rotor (Halbach-DSSR). Both designs are characterized by ultra-high rotor pole-to-stator coil ratios, as illustrated in Figs. 1 and 2, which enhance flux modulation capability and torque output. The stators in both machines comprise 12 primary teeth, each embedded with 2 auxiliary teeth to intensify flux harmonics and support effective torque production. This configuration is specifically tailored to strengthen the airgap flux density, thereby improving the machine's electromagnetic response.

In the spoke-DSSR model, the rotor employs a 40-pole spoke-type PM architecture, strategically designed to concentrate flux in the active airgap region. This approach significantly elevates torque density and overall efficiency by minimizing magnetic flux leakage and maximizing the utilization of PMs. In contrast, the Halbach-DSSR adopts a single-rotor design comprising back-to-back Halbach arrays, with the first rotor–stator pair rotated by 30 electrical degrees relative to the second, while in the spoke-type configuration, one of the stators is rotated by 4.5 electrical degrees. This rotation introduces spatial phase displacement, which enhances

TABLE I
Parameters and Dimentions of the Two Motors.

Specification	*Spoke-Type*	*Halbach Array*
Rated speed (rpm)	300	300
No. of rotor poles	40	40
No. of turns per phase	26	26
Airgap length (mm)	1.5	1.5
Stator outer diameter (mm)	300	300
Stator inner diameter (mm)	150	150
Stator yoke thickness (mm)	18	18
Stator pole width (mm)	45	45
PM volume (cm^3)	866	1910

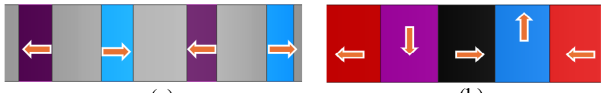

(a) (b)

Fig. 3. Arrangement of PMs. (a) Spoke-DSSR and (b) Halbach-DSSR.

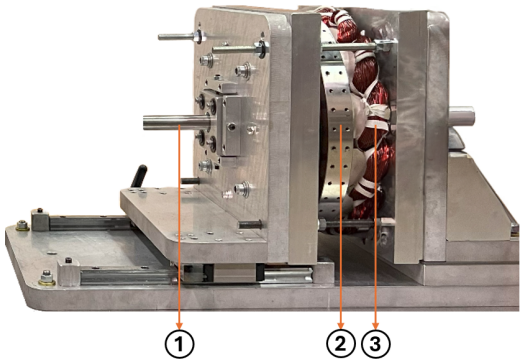

Fig. 4. The Spoke-SSSR prototype. (1) Shaft. (2) Spoke-type rotor. (3) Stator and three phase windings.

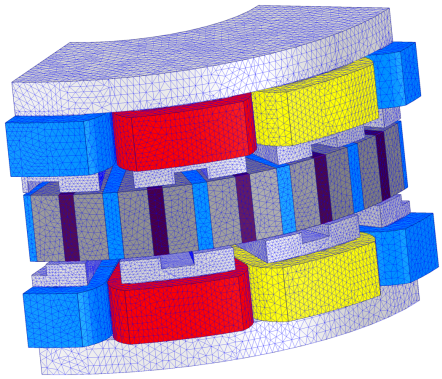

Fig. 5. Tetrahedral mesh elements of Spoke-DSSR.

magnetic coupling and smoothens torque waveform.

Moreover, the Halbach array rotors are separated by a decoupler, and its material composition plays a pivotal role in torque performance. Employing magnetized materials for the decoupler enhances the average torque output by approximately 13%. The Halbach array PM arrangement fosters an outward-directed magnetic field, allowing better field uniformity, reduced rotor disc thickness, and compact axial dimensions, making it favorable for applications demanding space-constrained integration. Although both rotors share the same number of poles, their structural and magnetic characteristics yield distinct performance outcomes, warranting a deeper evaluation of torque capability, efficiency, and implementation feasibility. The PM arrangements for both the Halbach array and the spoke-type configuration are shown in Fig. 3.

Both designs use a 12 slot stator and have 12 coils in a three-phase double layer configuration. These design can also operate with a three-phase single layer configuration, utilizing as few as six coils. This modular winding approach not only reduces design complexity and manufacturing cost but also facilitates scalable performance tuning [18]. The resulting flexibility supports the integration of advanced cooling techniques enabling the machines to operate with high current densities. Moreover, this adaptability permits variation in stator tooth count and rotor pole configurations, optimizing electromagnetic interactions for different application requirements and thermal constraints. The relationship between the rotor poles, main and auxiliary stator teeth, and armature poles is given by:

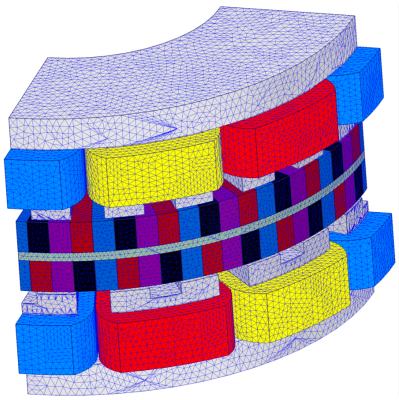

Fig. 6. Tetrahedral mesh elements of elements of Halbach-DSSR.

$$P_r = 2 \times T_{ms} \times t_{st} - P_a, \tag{1}$$

where P_r represents the number of rotor poles, T_{ms} the number of main stator teeth, t_{st} the number of auxiliary stator teeth, and P_a the number of armature poles.

The torque produced by the rotor and stator components is determined by calculating the tangential component of their surfaces. The tangential force acting on individual stator teeth and rotor components can be determined by integrating the stress across the corresponding mechanical elements as:

$$F_t = \int f_t(t,\theta) ds. \tag{2}$$

By evaluating the tangential force contributions over each segment of the stator and rotor, and multiplying by their radial displacement from the axis of rotation, an accurate tangential force density is achieved as:

$$f_t(t,\theta) = \frac{B_a(t,\theta) B_t(t,\theta)}{\mu_0}, \tag{3}$$

where $B_a(t,\theta)$ and $B_t(t,\theta)$ are the axial and tangential flux densities, respectively and μ_0 is the vacuum magnetic permeability. B_g is the airgap flux density. All three parameters can be obtained using FEA and employed for the derivation of the electromagnetic torque analysis as:

$$T_{em} = \frac{D_r g L_{stk}}{4\mu} \frac{\partial}{\partial \theta_r} \int_0^{2\pi} \left(B_{PM}(\phi,t) + B_R(\phi,t)\right)^2 d\phi, \tag{4}$$

where D_r is the average diameter, g the airgap, L_{stk} the stack length, B_{PM} the open-circuit airgap flux density, μ the magnetic permeability and B_R the armature airgap flux density [19]. The airgap magneto motive force (MMF) in open-circuit condition is given by:

$$F_{PM}(\phi') = F \frac{1}{2h+1} \sin[(2h+1) p_m \phi'], \tag{5}$$

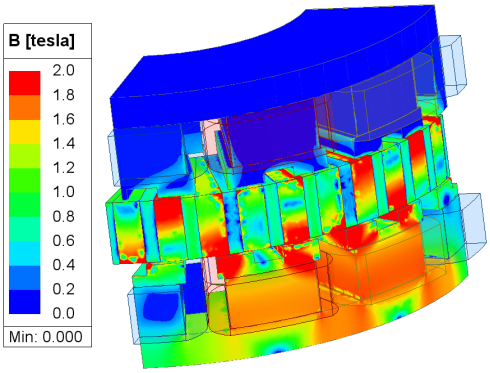

Fig. 7. Magnetic flux density of Spoke-DSSR.

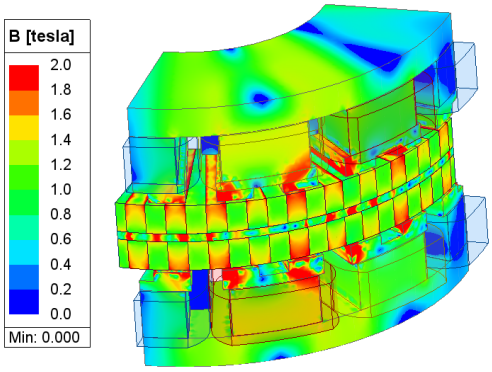

Fig. 8. Magnetic flux density of Halbach-DSSR.

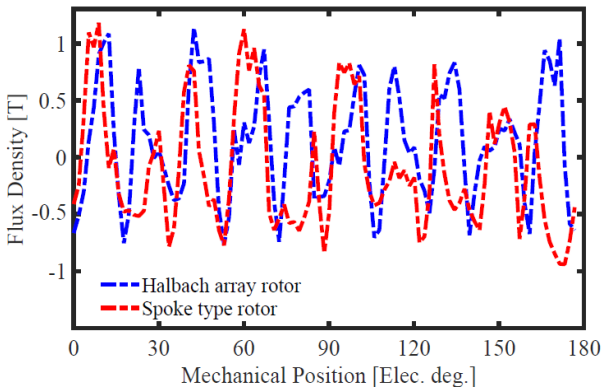

Fig. 9. The airgap flux density of Spoke-DSSR and Halbach-DSSR.

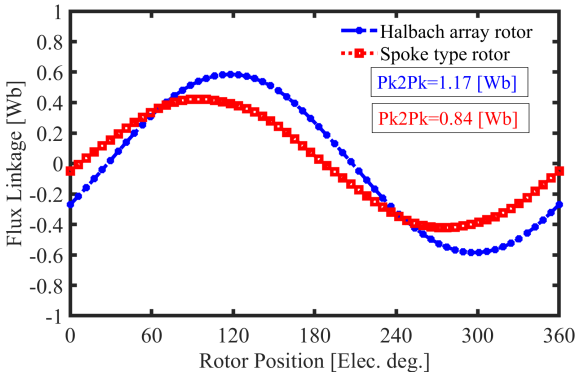

Fig. 10. Flux linkage comparison in AFPM vernier machines with spoke-type and Halbach array rotors.

where $(2h+1)p_m$ is the PM pole pair number, F is the amplitude of the force waveform and h is an integer harmonic index. The angular positions in the reference frames of the rotor and stator are related by:

$$\phi = \phi' + \theta_{r0} + \omega_r t, \tag{6}$$

where θ_r is the angle of the rotor relative to the stator, $\omega_r t$ is the angular position, and θ_{r0} is the initial position of the rotor with reference to the stator. The cogging torque arises due to the interaction between the PM on the rotor and the stator slot geometry, causing periodic variations in reluctance as the rotor rotates. The cogging torque can be calculated by the following:

$$T_{\text{cog}} = -\frac{1}{2}\psi_g^2 \frac{dR}{d\theta_r}. \tag{7}$$

III. Results and Discussion

This paper systematically compares Spoke-DSSR and Halbach-DSSR configurations, examining torque characteristics, torque ripple, airgap flux density, and harmonic content. The machine structure was modeled using Ansys Electronics Desktop 2024 R1 [20], validating 3D FEA simulations through analytical calculations and prototype testing of a single-stator spoke-type rotor (SSSR), shown in Fig. 4. The full prototype is in development, ensuring the model accurately reflects system specifications and operating conditions, while the Halbach-DSSR design undergoes refinement. The main parameters for these two machines are outlined in Table I.

The tetrahedral mesh structures used in the two models are depicted in Figs. 5 and 6, where each comprising approximately 850,000 mesh elements. The magnetic flux density distribution in the Spoke-DSSR and Halbach-DSSR topologies is shown in Figs. 7 and 8. In both configurations, the flux density within the rotor and auxiliary teeth exceeds 2T, indicating high levels of magnetic saturation.

The stator back iron of the Halbach-DSSR experiences greater flux density compared to the Spoke-DSSR, primarily because the latter concentrates flux on a single axial side. Additionally, the edge effects from the PMs intensify saturation at the stator core's inner and outer diameters in both machines. Notably, auxiliary teeth saturation in the Halbach-DSSR approaches that of the spoke-type machine, underscoring the importance of maintaining sufficient core thickness to mitigate over-saturation and associated iron losses.

The airgap flux density for both machines as illustrated in Fig. 9, reveals the distinct profiles shaped by their respective magnet configurations. Fig. 10 compares the flux linkage of both designs, showing that the Halbach array generates a higher peak-to-peak flux linkage of 1.17Wb, while the spoke-

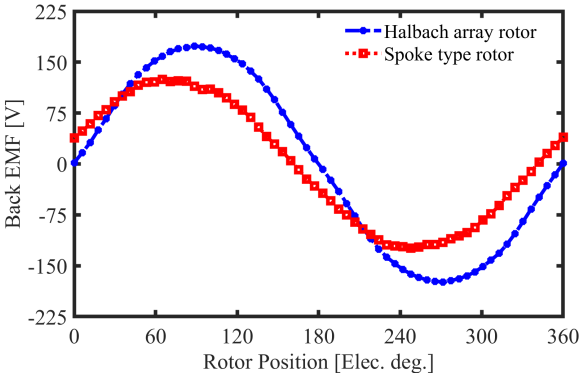

Fig. 11. Back-EMF at the rated speed

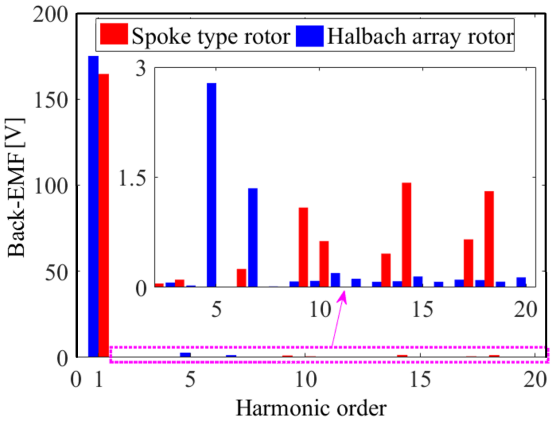

Fig. 12. Harmonic spectra of the back-EMF waveform.

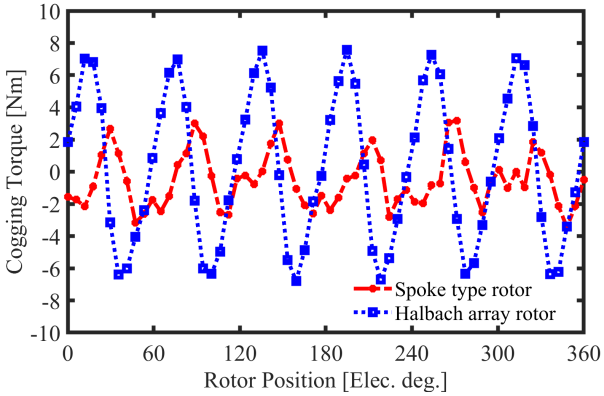

Fig. 13. Cogging torque profile of the proposed motors.

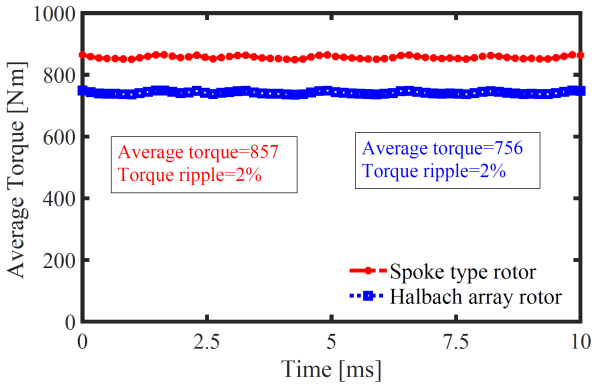

Fig. 14. Torque for the two topologies.

type machine achieves 0.84Wb. This elevated flux linkage in the Halbach configuration contributes to stronger back electromotive force (BEMF) under no-load conditions, as depicted in Fig. 11, where the peak back-EMF for Halbach-DSSR is 175V versus 120V in Spoke-DSSR.

The harmonic spectra of the back-EMF waveform (Fig. 12) reveals that the Halbach-DSSR topology induces more prominent higher-order harmonics. In comparison, the Halbach rotor demonstrates a marginally higher total harmonic distortion (THD) of 1.25% versus 1.21% for the Spoke rotor, primarily due to a dominant 5th harmonic component. Both rotor configurations exhibit low THD levels, indicative of stable back-EMF profiles and smooth operational characteristics. These components elevate torque ripple, increase iron losses, and complicate control strategies.

The impact of magnetic slot interaction on cogging torque is quantified in Fig. 13, where the Halbach-DSSR exhibits a peak-to-peak cogging torque of 14Nm twice as high as that of the Spoke-DSSR (7Nm). The Halbach array higher cogging torque is the result of a more intense interactions between the PMs and stator slot openings. The average electromagnetic torque values of the spoke-type and Halbach array rotors are 857Nm and 756Nm, respectively, as depicted in Fig. 14, which also shows both machines maintain a low torque ripple of approximately 2%. This indicates the superior torque-producing capability of the spoke-type machine, especially in applications requiring high torque density and stable output.

The electromagnetic torque increases approximately linearly in both machines, with the Spoke-DSSR consistently providing higher torque across all current densities, as shown in Fig. 15. The superior performance of Spoke-DSSR becomes even more pronounced under high electrical loading conditions, reaffirming the spoke-type typology's suitability for demanding direct-drive applications.

Table II provides a comprehensive comparison between Spoke-DSSR and Halbach-DSSR motor designs under varying current densities (J = 3.5, 17.5, and 35A/mm²), evaluating key parameters such as torque output, torque ripple, power loss components, and efficiency indicators. As observed, torque increases with current density for both configurations, but the Spoke-DSSR consistently delivers higher torque across all operating points. For instance, at 35A/mm², it reaches 857Nm compared to 756Nm for the Halbach-DSSR. Moreover, both machines demonstrate a torque ripple of approximately 2%, with the innovative designs maintaining this minimal ripple even under high current density conditions highlighting their superior operational smoothness. This enhanced torque capability comes at the cost of increased core and copper losses,

TABLE II
COMPARISON OF SPOKE-DSSR AND HALBACH-DSSR MOTOR DESIGN. BOLD VALUES HIGHLIGHT THE HIGHEST-PERFORMING OF BOTH MOTORS UNDER EACH OPERATING CONDITION, FACILITATING DIRECT COMPARISON ACROSS CONFIGURATIONS.

Design	**J**	**Axial Length**	**Torque**	**T-Ripple**	**Power**	**Core Loss**	**Copper Loss**	**Kt**	**Goodness**	**Specific Torque**	**Torque Density**
	(A/mm^2)	(mm)	(Nm)	(%)	(W)	(W)	(W)	($Nm/(A/mm^2)$)	($Nm/\sqrt{W_{loss}}$)	(Nm/Kg)	(Nm/L)
Spoke-DSSR	3.5	142	97	8	3,047	32	38	27.7	11.6	15.2	12.9
Halbach-DSSR	3.5	147	78	39	2,463	55	38	22.4	8.1	5.6	10.1
Spoke-DSSR	17.5	142	471	3	14,787	100	948	26.9	14.5	73.6	62.5
Halbach-DSSR	17.5	147	387	8	12,151	67	948	22.1	12.1	27.4	49.5
Spoke-DSSR	35	142	**857**	**2**	26,923	190	3,794	24.5	13.6	**134.1**	**113.8**
Halbach-DSSR	35	147	756	**2**	23,735	**109**	3,794	21.6	12.1	53.6	96.9

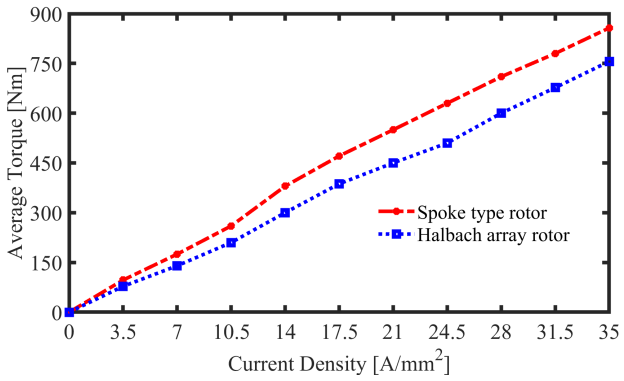

Fig. 15. Torque versus current density.

particularly at higher current densities, where Spoke-DSSR registers 190W and 3794W, respectively. However, despite the higher losses, the Spoke-DSSR maintains a better torque-to-loss efficiency, as reflected in its higher goodness factor and specific torque.

The torque constant (K_t) further reinforces the Spoke-DSSR's advantage, showing higher or comparable values across all cases, indicating a stronger torque production capability per unit current density. In terms of torque density, a critical metric for space-constrained applications, the Spoke-DSSR design shows remarkable performance, achieving 113.8Nm/L at 35A/mm², which is about 17% higher than the Halbach-DSSR (96.9Nm/L). These performance suggest that the Spoke-DSSR motor leverages its PM material and geometry more efficiently, making it particularly compatible for high-performance applications demanding high torque output, minimal ripple, and superior efficiency.

IV. CONCLUSION

This study conducted a comprehensive comparative analysis of two dual-stator axial-flux permanent magnet (AFPM) vernier machines: a spoke-type rotor and a back-to-back Halbach array configuration. Using three-dimensional finite element analysis (3D FEA), validated utilizing a laboratory prototype, key electromagnetic metrics including torque density, torque ripple, goodness factor, airgap flux distribution, and efficiency were evaluated.

The results revealed that the spoke-type rotor consistently outperformed the Halbach-DSSR across multiple indices, notably in power density and torque ripple suppression, which underscored its suitability for low-speed direct-drive applications. Under a current density of 35A/mm², the spoke-type machine reached an efficiency of 85.2%, compared to 83.5% for its Halbach counterpart.

Furthermore, the spoke-type configuration delivered an average torque approximately 13.5% higher than that of the Halbach-type (857Nm compared to 756Nm), while both topologies demonstrated a torque ripple of approximately 2%, reinforcing their smooth electromagnetic performance. The spoke-type DSSR also demonstrated an extended constant power operation range, which was attributed to its enhanced flux concentration capability. Although the Halbach-DSSR utilized a greater volume of PM material, the spoke-type topology delivered superior overall electromagnetic performance.

REFERENCES

[1] M. Wang, D. Li, and R. Qu, "Analysis of an axial-flux slotted limited-angle torque motor with quasi-halbach array for torque performance improvement," *CES Transactions on Electrical Machines and Systems*, vol. 7, no. 3, pp. 266–274, September 2023.

[2] W. Liu, J. Wang, and T. A. Lipo, "A consequent pole single rotor single stator vernier design to effectively improve torque density of an industrial pm drive," *IEEE Transactions on Industrial Electronics*, vol. 70, no. 1, pp. 255–264, 2023.

[3] A. Mohammadi, A. M. Cramer, and D. M. Ionel, "Comparative Analysis of Vernier Machines with Spoke, Surface Mounted, and Halbach PM Rotors for In-wheel Traction," in *2024 IEEE Transportation Electrification Conference and Expo (ITEC)*, 2024, pp. 1–6.

[4] E. Mohammadi, A. Mohammadi, M. A. J. Kondelaji, P. Asef, and D. M. Ionel, "Innovative dual-excitation drive in fault tolerant double-stator vernier machines for ship propulsion," in *Proceedings of the IEEE Energy Conversion Congress and Exposition (ECCE)*. Birmingham, UK: IEEE, August 2025.

[5] R. Tu, H. Yang, H. Lin, H. Zhan, L. Chen, W. Chen, D. Wu, and M. Yu, "Electromagnetic-thermal coupled design of halbach-array axial-flux pm machine for direct-drive automated guided vehicle," *IEEE Transactions on Transportation Electrification*, vol. 11, no. 1, pp. 2097–2107, February 2025.

[6] G. Yang, J. Li, and M. Lin, "Design and analysis of novel modular stator axial-flux permanent magnet vernier machine with improved power factor," *IEEE Access*, vol. 11, pp. 108 580–108 590, 2023.

[7] V. Rallabandi, P. Han, M. G. Kesgin, N. Taran, and D. M. Ionel, "Axial-field vernier-type flux modulation machines for low-speed direct-drive applications," *2019 IEEE Energy Conversion Congress and Exposition (ECCE)*, pp. 3123–3128, 2019.

[8] H. Chen, N. A. Demerdash, A. M. El-Refaie, Y. Guo, W. Hua, and C. H. Lee, "Investigation of a 3d-magnetic flux pmsm with high torque density for electric vehicles," *IEEE Transactions on Energy Conversion*, vol. 37, no. 2, pp. 1442–1454, 2021.

[9] Z. Shi, X. Sun, Z. Yang, Yingfeng, G. Lei, J. Zhu, and C. H. T. Lee, "Design optimization of a spoke-type axial-flux pm machine for in-wheel drive operation," *IEEE Transactions on Transportation Electrification*, vol. 10, no. 2, pp. 3770–3781, June 2024.

[10] Y. Lu, Y. Kai, S. Songjun, L. Yixiao, X. Fei, and L. Cheng, "Study on the influence of a combined-halbach array for the axial flux permanent magnet electrical machine with yokeless and segmented armature," *IEEE Transactions on Magnetics*, vol. 60, no. 3, pp. 1–5, March 2024.

[11] S. Cai, J. L. Kirtley, and C. H. T. Lee, "Critical Review of Direct-Drive Electrical Machine Systems for Electric and Hybrid Electric Vehicles," *IEEE Transactions on Energy Conversion*, vol. 37, no. 4, pp. 2657–2668, 2022.

[12] L. Wu and Z. Tian, "Analysis of a triple-stator axial-flux spoke-type permanent magnet vernier machine," *IEEE Transactions on Industry Applications*, vol. 58, no. 5, pp. 6024–6034, September-October 2022.

[13] M. Bilal, J. Ikram, A. Fida, S. S. H. Bukhari, N. Haider, and J. Ro, "Performance improvement of dual stator axial flux spoke type permanent magnet vernier machine," *IEEE Access*, vol. 9, pp. 64 179–64 188, 2021.

[14] P. Srikhumphun, S. Sangswang, C. Pothisarn, and S. Rajakaruna, "Design optimization and comparative study of skewed halbach-array magnets torus axial-flux permanent magnet motors for electric vehicles," *IEEE Access*, vol. 12, pp. 99 912–99 920, 2024.

[15] P. Asef, R. B. Perpina, M. R. Barzegaran, and A. Lapthorn, "Multiobjective design optimization using dual-level response surface methodology and booth's algorithm for permanent magnet synchronous generators," *IEEE Transactions on Energy conversion*, vol. 33, no. 2, pp. 652–659, November 2018.

[16] D. M. Ionel, D. Jackson, G. Starr, and A. Turner, "Permanent magnet brushless motors for industrial variable speed drives," in *2002 International Conference on Power Electronics, Machines and Drives (Conf. Publ. No. 487)*. IET, 2002, pp. 650–654.

[17] T. Okita and H. Harada, "3-d analytical model of axial-flux permanent magnet machine with segmented multipole-halbach array," *IEEE Access*, vol. 11, pp. 2078–2091, 2023.

[18] L. Cao, Y. Zuo, S. Xie, C. C. Hoang, B. S. Han, and C. H. T. Lee, "Comparative study of permanent-magnet vernier motor and interior permanent-magnet motor for hybrid electric vehicles," *IEEE Transactions on Industry Applications*, vol. 59, no. 6, pp. 6601–6614, 2023.

[19] L. Wu and R. Qu, "A novel dual-stator vernier permanent magnet machine with improved power factor," *IEEE Transactions on Industry Applications*, vol. 58, no. 3, pp. 3486–3496, 2022.

[20] Ansys® Electronics Desktop, "Maxwell, version 24.1," 2024, ANSYS, Inc.